

# A Novel Minimum Distance Constraint Method Enhanced Dual-Foot-Mounted Inertial Navigation System for Pedestrian Positioning

Tao Liu<sup>ID</sup>, Jian Kuang<sup>ID</sup>, You Li<sup>ID</sup>, *Member, IEEE*, and Xiaoji Niu<sup>ID</sup>

**Abstract**—Foot-mounted inertial navigation system (Foot-INS) with the zero velocity update (ZUPT) has become one of the indispensable technical means in professional pedestrian positioning fields due to the advantages of self-constraint and immune to environmental factors. The dual-Foot-INS can provide more excellent autonomous positioning performance than a single-Foot-INS because it utilizes more opportunities for zero velocity correction and additional distance constraint information. However, the classical dual-Foot-INS does not fully exploit the distance constraint potential for positioning improvement. In this article, we proposed a novel minimum distance constraint (MDC) method that achieves higher positioning accuracy than the traditional dual-Foot-INS methods. To obtain an accurate and consistent state estimation under the nonlinear distance constraint problem, we propose an iterative distance constraint (IDC) algorithm. The IDC is transformed into an approximate linear constraint model, and an alternative estimate is obtained by the estimation projection method. To solve the problem that the distance constraint moment in the traditional method is affected by the recursive foot positions, we propose a more reasonable and reliable minimum distance moment detection (MDMD) method. The proposed MDMD method maximizes the positioning performance improvement of the dual-foot pedestrian system. Two rigorous experimental tests with a long walking trajectory without turn around and closed loop were conducted to verify the effectiveness of the proposed method, the positioning error of the proposed method is reduced by 83.5% and 62.9% compared to the classical ZUPT and MDC methods, respectively.

**Index Terms**—Distance constraint algorithm, foot-mounted inertial navigation system (Foot-INS), pedestrian positioning system, zero velocity update (ZUPT).

## I. INTRODUCTION

LOCATION-BASED services (LBSs) are attracting tremendous attention owing to their highly potential applications facilitating peoples' lifestyles and boosting

Manuscript received 22 February 2023; accepted 25 April 2023. Date of publication 28 April 2023; date of current version 25 September 2023. This work was supported in part by the National Key Research and Development Program of China under Grant 2016YFB0502202, and in part by the Special Fund of Hubei LuoJia Laboratory under Grant 220100007. (Corresponding authors: Xiaoji Niu; Jian Kuang.)

Tao Liu and Jian Kuang are with the GNSS Research Center, Wuhan University, Wuhan 430072, Hubei, China (e-mail: liu\_tao@whu.edu.cn; kuang@whu.edu.cn).

You Li is with the State Key Laboratory of Information Engineering in Surveying, Mapping and Remote Sensing and the Hubei LuoJia Laboratory, Wuhan University, Wuhan 430072, Hubei, China (e-mail: liyou@whu.edu.cn).

Xiaoji Niu is with the GNSS Research Center, the Artificial Intelligence Institute, and the Hubei LuoJia Laboratory, Wuhan University, Wuhan 430072, Hubei, China (e-mail: xjniu@whu.edu.cn).

Digital Object Identifier 10.1109/JIOT.2023.3271309

functionalities in smart cities [1], [2], [3]. Recently, pedestrian positioning has been the focus of many research efforts as the core supporting technology of LBS [2], [3], [4], [5], [6], [7], [8], [9]. The global navigation satellite system (GNSS) is capable of providing fast and reliable positioning services for pedestrians in most outdoor environments. However, the efficiency of GNSS techniques is strongly hindered in sheltered outdoors and indoor environments [5], [6]. For this, various alternative solutions have been proposed so far using WiFi, Bluetooth, radio frequency identification (RFID), acoustics, Infrared, ultrawideband (UWB), magnetic fields, or inertial measurement units (IMUs), to provide pedestrian position information in indoor environments [3], [5], [8]. Unlike other commonly used technologies, such as wireless signals or vision sensors, inertial-based dead-reckoning (DR) is completely self-contained. It exhibits a series of interesting features, including high-short-term positioning accuracy, and independent of infrastructure and conditions, such as non-line-of-sight, ambient light, and abnormal electromagnetic interferences. The inertial-based DR solution is the most promising and feasible pedestrian positioning approach in complicated and changeable indoor or satellite-unavailable scenarios. It presents a highly interesting potential for applications, such as locating and monitoring emergency responders in forest fires, residential building fires, or earthquake disasters [3], [10], [11].

The inertial-based solution faces the problem of rapid accumulation of positioning errors due to sensor errors [3], [12], [13]. Therefore, the zero-velocity update (ZUPT) algorithm-based foot-mounted inertial navigation system (Foot-INS) has been proposed [14] for pedestrian positioning applications. During the stance phase, the foot is in contact with the ground and the velocity of the foot is zero [15], [16]. The ZUPT algorithm corrects the error of the INS using the zero velocity during the stance phase and the Kalman filter (KF). The ZUPT-based Foot-INS has demonstrated its capability to mitigate the divergence speed of positioning errors. Unfortunately, the heading error and the vertical gyro bias in the ZUPT algorithm have been proved unobservable [17], [18]. Researchers have proposed many methods to enhance the performance of ZUPT-based Foot-INS, such as the angular rate update algorithm [19], the straight-line constraint method [20], [21], the body odometer model [22], and the building's structural characteristics approach [23]. However, the above methods must satisfy their

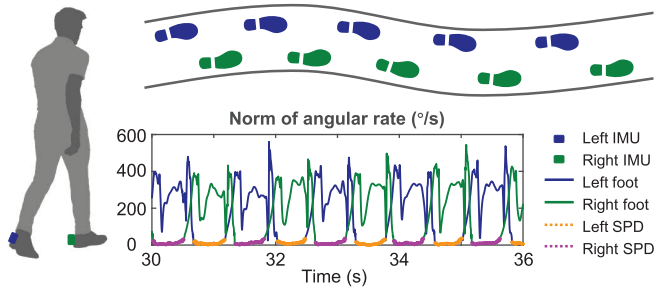


Fig. 1. Dual-foot pedestrian positioning. A walking test with about 1.2 m/s speed illustrates that the number of the stance phase epochs is approximately 75% of the total epochs, while the ratio is about 37% in single-foot solution. SPD represents the SPD statistics.

respective specific assumptions to be helpful. Furthermore, these assumptions do not represent the regular motion characteristic signals during walking.

The dual-foot-mounted inertial sensors solution presents an alternative to further improve the autonomous positioning capability compared to the single-foot solution [24]. As shown in Fig. 1, the ratio of the elapsed time in the stance phase to the total walking time in the dual-foot pedestrian system is about twice that of the single-foot solution. Therefore, the inherent double zero-velocity information can benefit from establishing a model using the link between the left and right foot. Usually, the distance information is used to establish the link between the feet. Two main classification strategies defined the research work on dual-foot pedestrian systems: using or not using an additional ranging sensor [25]. In the ranging-sensor-based solution, a pair of ultrasonic sensors (e.g., sonar) [24], [26], [27] or visual devices (e.g., camera) [28], [29], [30], are mounted on the left and right foot to measure the distance between them. However, the ranging-sensor-based solution is unsuitable for ubiquitous pedestrian positioning applications due to the need for a specialized platform, high-hardware cost, and high-system complexity.

In the self-constrained dual-foot solution (i.e., without the assistance of a ranging sensor), the maximum distance constraint is the earliest proposed algorithm. This approach assumes an upper bound for the distance between the two systems [31]. Once the relative distance between feet exceeds this upper bound, the latter is used as an observation to correct the system. The maximum distance constraint idea was also utilized in [32]. In addition, the relative position vector of any foot at the standing ending phase is modeled as a constant to improve the positioning performance [33]. Nevertheless, this method is only suitable for straight line walking scenarios. The work in [34] proposed an inverted pendulum model to estimate the relative position vector in the body frame between the two foot-mounted sensors. Due to the heading angle divergence, there will be errors in the relative position vector derived by the inverted pendulum model after attitude rotation. In [35], a comprehensive dual-foot positioning solution was proposed using the maximum distance constraint, the maximum step length constraint of a single foot, and the straight line constraint algorithms. The maximum distance between feet is constantly changing with the variation in walking speed and

mode. The minimum distance between feet has manifested as a constant in most walking scenarios, showing better stability than the maximum distance. Therefore, the minimum distance constraint (MDC) algorithm is proposed [36], which uses the constant minimum distance between the dual-foot-mounted IMUs to enhance pedestrian positioning. The MDC idea applied in this study benefits from its strong stability.

An accurate and reasonable distance constraint moment is essential to ensure positioning performance and reliability in the self-constrained dual-foot pedestrian system. Almost all current self-constrained systems [31], [32], [35], [36] use recursive left and right foot positions to determine when to execute the distance constraint algorithm. However, the errors in the recursive positions are divergent and thus gradually increase with walking time, resulting in an unreasonable determination of the distance constraint moment. It also leads to a complete inconsistency between the estimated distance and the actual fluctuations between the left and right foot. Note that although the distance constraint moment introduces errors in the current dual-foot pedestrian systems, it still improves the positioning performance compared to the single-foot solution. Therefore, a distance constraint moment detection method that is independent of the recursive positions is needed for the dual-foot pedestrian system.

The distance constraint optimal estimation is also crucial for the dual-foot pedestrian system. The pseudo-observation approach is a classical strategy [27], [35], [36]. This approach considers the distance constraint as an additional observation and combines it with the original measurement model (e.g., ZUPT) to construct an augmented measurement model. Due to the nonlinearity of the augmented measurement model, nonlinear filtering algorithms (e.g., the extended KF (EKF) [27], [36], the unscented KF (UKF) [37], [38], and the cubature KF (CKF) [39], [40]) can be used to solve the distance constraint problem. The quadratic constraint method is also used to solve the distance constraint problem. This method considers the distance constraint as a conditional extremum problem of minimum state variance under the quadratic constraint condition [31], [41], [42]. However, the quadratic constraint algorithm necessitates high-computational complexity and lacks a rigorous covariance matrix estimation. Although the approximate covariance matrix has been derived in [31], it suffers from numerical instability. Therefore, an accurate, consistent, and low-complexity distance constraint algorithm is valuable for the dual-foot pedestrian system.

The autonomous positioning performance of the previous dual-foot pedestrian positioning systems is not fully unleashed. On the one hand, in the distance constraint optimal estimation, the quadratic constraint algorithm [31], [41] encounters the confusion of inconsistency between the covariance matrix and the system state, and the pseudo-observation approach [27], [30], [36] faces the problem of insufficient estimation accuracy and low scalability. On the other hand, in the constraint moment determination [31], [32], [35], [36], the current methods are subject to the recursive position error divergence, resulting in an incorrect constraint moment.

In this study, we propose a novel enhanced MDC method for the dual-foot pedestrian system. The proposed MDC method

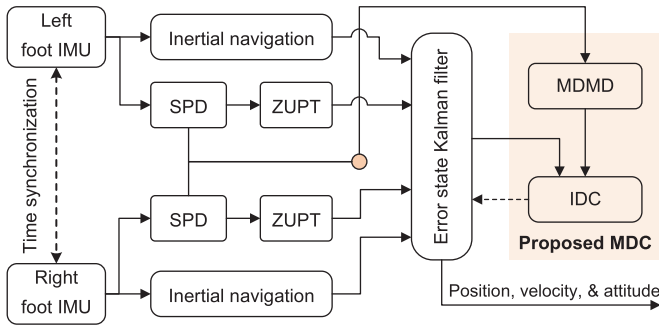


Fig. 2. Proposed MDC for the dual-foot pedestrian positioning system. SPD represents SPD. The system state and the corresponding covariance matrix estimated by the proposed MDC method are used to update the error state KF.

performs accurate and consistent state estimation. In addition, the proposed method solves the problem that the constraint moment is affected by the recursive position drift, and has an appropriate constraint moment. Compared with the previous approaches, the proposed method fully exploits the potential of MDC in the dual-foot pedestrian system and significantly improves autonomous positioning performance. The proposed method is expected to continuously and effectively improve the autonomous positioning capability in most normal walking scenarios. The contributions of this article are summarized as follows.

- 1) We propose an iterative distance constraint (IDC) algorithm in the KF framework. The IDC enables accurate and consistent state estimation under the nonlinear distance constraint problem. Moreover, the IDC has the advantage of low-computation complexity.
- 2) We observed a new phenomenon between the minimum distance moment and the stance phase based on statistical analysis. Then, we designed a minimum distance moment detection (MDMD) method using the newly discovered phenomenon. The MDMD is independent of the recursive positions. Therefore, it improves the precision of the MDMD, reduces the algorithm complexity, and allows a more reasonable and accurate position estimate compared to classical methods.
- 3) We have comprehensively evaluated the proposed method through rigorous experimental tests with a long walking trajectory without turn around and closed loop, and demonstrated the effectiveness of the proposed method.

The remainder of this article is organized as follows. An overview of the proposed method is provided in Section II. In Section III, we describe the basic part of the proposed method, and present the IDC algorithm. Section IV describes the phenomenon between the minimum distance moment and the stance phase, and provides the MDMD method. Section V presents the experimental results and relevant comparative analysis to traditional methods. Finally, Section VI summarizes and concludes this article.

## II. SYSTEM OVERVIEW

Fig. 2 shows that a reliable IMU data acquisition is necessary for the proposed dual-foot pedestrian positioning method.

TABLE I  
MAIN CHARACTERISTICS OF THE MEMS INERTIAL MODULE

Parameters	Gyroscope	Accelerometer
Data rate	200 Hz	200 Hz
Dynamic range	2000 °/s	16 g
Bias instability	10 °/h	0.2 mg
White noise	0.24 °/√h	0.06 m/s/√h
Weight		≈ 50 g
Size (no shell)		32 × 25 × 12 mm
Battery power	continuous work for more than 10 hours	

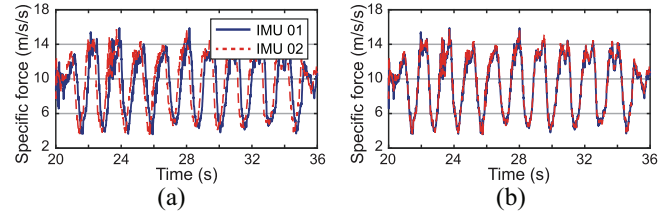


Fig. 3. Bluetooth-based time synchronization. Two inertial sensors were mounted on a flat plate to perform the same movement process. The time differences between the two sensors before and after the time synchronization operation are 170 and 5 ms, respectively. (a) Before time synchronization. (b) After time synchronization.

The essential component of the proposed method includes ZUPT-based Dual-Foot-INS and KF-based state estimation. The straightforward and elegant MDMD and the effective IDC algorithms are the unique attributes of the proposed MDC method that distinguish it from previous ones.

During the data acquisition process, two compact inertial modules were required to be tightly attached to the heels of the pedestrian's right and left shoes to obtain stable and high-quality IMU data. The two inertial modules used in this study had the same accuracy level. The inertial module consists of a low-cost MEMS IMU, power supply module, low-energy Bluetooth module, data storage module, and a general multiprotocol system-on-chip [43]. The technical characteristics of the inertial module are summarized in Table I. Moreover, a smartphone app was used to control the start and end of the inertial modules via Bluetooth signal, similar to the app reported in our previous work [23].

Time synchronization of the multiple inertial sensors is critical for the proposed method. For this, Bluetooth signals exchanged between smartphones and inertial sensors were used to obtain the time difference between the multiple devices. Then, the data sensed from the multiple inertial sensors are unified under the same time system using linear interpolation. To verify the accuracy of the Bluetooth-based time synchronization scheme, we mounted multiple inertial sensors on a flat panel and performed the same motion simultaneously. The time synchronization accuracy is better than 10 ms based on numerous experimental tests. Therefore, we demonstrate that it can meet the accuracy requirements of the dual-foot pedestrian system. Fig. 3 illustrates the Bluetooth-based time synchronization scheme.

## III. DUAL-FOOT PEDESTRIAN POSITIONING

In this section, we first introduce the necessary components of the proposed dual-foot pedestrian positioning method,

i.e., the inertial navigation algorithm and the stance phase detection (SPD). Then, the state space and ZUPT models are constructed. Finally, we propose the novel MDC algorithm and analyze its computational complexity.

### A. Inertial Navigation Algorithm

The primary principle of the INS is to use the previous recursive navigation state (i.e., position, velocity, and attitude), incorporated with the angular rate and specific force measurements, to calculate the current navigation state of the foot through numerical integration [13]. We used the well-known north-east-down geographic coordinate system and the front-right-down coordinate system as the navigation coordinate frame (i.e.,  $n$  frame) and the body coordinate frame (i.e.,  $b$  frame), respectively. The coordinate systems are defined in detail in [44]. The components related to the Earth's rotation are neglected [23] due to considerable noise in the angular rate measured by the MEMS inertial sensor.

The attitude matrix  $C_b^n$ , velocity  $v_k^n$ , and position  $r_k^n$  update processes are given as follows:

$$C_{b,k}^n = C_{b,k-1}^n \left[ \mathbf{I} + \frac{\sin \rho}{\rho} [\boldsymbol{\rho} \times] + \frac{1 - \cos \rho}{\rho^2} [\boldsymbol{\rho} \times]^2 \right] \quad (1)$$

$$v_k^n = v_{k-1}^n + C_{b,k-1}^n v_{sf} + \mathbf{g}^n \Delta t \quad (2)$$

$$r_k^n = r_{k-1}^n + 0.5(v_{k-1}^n + v_k^n) \Delta t \quad (3)$$

where  $\boldsymbol{\rho} \approx \boldsymbol{\alpha}_k + (1/12)\boldsymbol{\alpha}_{k-1} \times \boldsymbol{\alpha}_k$  is the rotation vector associated with angular rate;  $\rho$  is the magnitude of  $\boldsymbol{\rho}$ ;  $\boldsymbol{\alpha}_k \approx \tilde{\boldsymbol{\omega}}_k^b \Delta t$ , with  $\tilde{\boldsymbol{\omega}}_k^b$  being the angular rate after removal of the gyroscope biases;  $v_{sf} \approx \boldsymbol{\gamma}_k + (1/2)\boldsymbol{\alpha}_k \times \boldsymbol{\gamma}_k + (1/12)(\boldsymbol{\alpha}_{k-1} \times \boldsymbol{\gamma}_k + \boldsymbol{\gamma}_{k-1} \times \boldsymbol{\alpha}_k)$  is the rotation vector associated with the specific force;  $\boldsymbol{\gamma}_k \approx \tilde{\mathbf{f}}_k^b \Delta t$ , with  $\tilde{\mathbf{f}}_k^b$  being the specific force after removal of the accelerometer biases;  $\mathbf{g}^n = [0 \ 0 \ g]^T$ , with  $g$  being the gravitational acceleration; and  $\Delta t$  is the sampling interval.

In the dual-foot pedestrian system, the tester needs to stand stationary for a few seconds. The initial gyroscope biases can be estimated by averaging the angular rate measurements in the stand stationary phase. Moreover, the initial roll and pitch angle can be calculated by incorporating the specific force and local gravity [45].

### B. Stance Phase Detection

An accurate and robust SPD algorithm is the kernel for the proposed dual-foot pedestrian positioning. The well-known generalized likelihood ratio test (GLRT) algorithm [16] exhibits excellent performance in most normal walking scenarios. This approach relies on the hypothesis that the measured specific force in the stance phase is the gravitational acceleration projection on the  $b$  frame and that the sensed angular rate is theoretically zero. The GLRT algorithm was used to detect the stance phase of the left and right foot, with a detection window size and threshold set as 5 and 6000, respectively.

A small number of abnormal detected points are inevitable in the GLRT, even in normal walking [23], [46]. Therefore, we use the approach in our previous work [23] to eliminate the abnormal non-zero-velocity points during the stance phase and the abnormal zero-velocity points during the swing phase. This

approach has been demonstrated to improve the reliability and accuracy of the GLRT algorithm by using an objective law that the gait phase (swing or stance phase) is continuous during a period of time in normal walking.

### C. State-Space Construction and ZUPT Model

We define the error state of position and velocity as the estimated state  $\hat{\mathbf{x}}$ , subtracting the true state  $\mathbf{x}$ , i.e.,  $\delta \mathbf{x} = \hat{\mathbf{x}} - \mathbf{x}$ , where  $\mathbf{x}$  can represent  $r^n$  and  $v^n$ . The attitude error  $\boldsymbol{\phi}$  is defined as  $\hat{C}_b^n = [\mathbf{I}_3 - (\boldsymbol{\phi} \times)] C_b^n$ , where  $\hat{C}_b^n$  and  $C_b^n$  are the estimated and true attitude matrices, respectively. The measured inertial signal is modeled as the sum of true signal, sensor biases, and white noise. The gyroscope biases  $\mathbf{b}_g$  and accelerometer biases  $\mathbf{b}_a$  can be modeled as a first-order Markov process. Moreover, the Earth's rotational components are neglected and explained in Section III-A. The system state of a single inertial system is defined as follows:

$$\delta \mathbf{x}_s = \left[ (\delta r^n)^T \quad (\delta v^n)^T \quad \boldsymbol{\phi}^T \quad \mathbf{b}_g^T \quad \mathbf{b}_a^T \right]^T. \quad (4)$$

The continuous-time dynamic model of the single inertial system is derived as follows:

$$\delta \dot{\mathbf{x}}_s = \mathbf{F}_s \delta \mathbf{x}_s + \mathbf{W}_s \quad (5)$$

$$\mathbf{F}_s = \begin{bmatrix} \mathbf{0}_3 & \mathbf{I}_3 & \mathbf{0}_3 & \mathbf{0}_3 & \mathbf{0}_3 \\ \mathbf{0}_3 & \mathbf{0}_3 & \mathbf{f}^n \times & \mathbf{0}_3 & C_b^n \\ \mathbf{0}_3 & \mathbf{0}_3 & \mathbf{0}_3 & -C_b^n & \mathbf{0}_3 \\ \mathbf{0}_3 & \mathbf{0}_3 & \mathbf{0}_3 & \mathbf{M}_g & \mathbf{0}_3 \\ \mathbf{0}_3 & \mathbf{0}_3 & \mathbf{0}_3 & \mathbf{0}_3 & \mathbf{M}_a \end{bmatrix}; \quad \mathbf{W}_s = \begin{bmatrix} \mathbf{0} \\ C_b^n \mathbf{w}_a \\ -C_b^n \mathbf{w}_g \\ \mathbf{w}_{bg} \\ \mathbf{w}_{ba} \end{bmatrix} \quad (6)$$

where  $\mathbf{f}^n = C_b^n \mathbf{f}^b$  is the specific force projection on the  $n$  frame;  $\mathbf{M}_g = \text{diag}([\tau_{bg} \ \tau_{bg} \ \tau_{bg}])$ ;  $\mathbf{M}_a = \text{diag}([\tau_{ba} \ \tau_{ba} \ \tau_{ba}])$ ;  $\tau_{ba}$  and  $\tau_{bg}$  are the correlation times, which are set to 1800 s;  $\mathbf{W}_s$  is the system noise, which is assumed to be zero-mean Gaussian white noise with the correlation covariance matrix  $\mathbf{Q}_s$ ;  $\mathbf{w}_a$  and  $\mathbf{w}_g$  are the measurement white noises of the accelerometer and gyroscopes, respectively; and  $\mathbf{w}_{ba}$  and  $\mathbf{w}_{bg}$  are the driving white noises of the bias model.

By discretizing the continuous-time dynamics model (5), we can obtain a discrete-time dynamics model for a single inertial system as follows:

$$\delta \mathbf{x}_{s,k} = \Phi_{k,k-1}^s \delta \mathbf{x}_{s,k-1} + \mathbf{w}_{s,k-1} \quad (7)$$

$$\begin{cases} \Phi_{k,k-1}^s = \exp[\mathbf{F}_{s,k-1} \Delta t] \approx \mathbf{I} + \mathbf{F}_{s,k-1} \Delta t \\ \mathbf{Q}_{s,k} \approx 0.5 \left[ \Phi_{k,k-1}^s \mathbf{Q}_s (\Phi_{k,k-1}^s)^T + \mathbf{Q}_s \right] \Delta t \end{cases} \quad (8)$$

where  $\Phi_{k,k-1}^s$  is the discrete transform matrix, and  $\mathbf{Q}_{s,k}$  is the covariance matrix of the discrete system noise  $\mathbf{w}_{s,k-1}$ .

In the dual-foot pedestrian system, a centralized KF is used to estimate the navigation state of the left and right foot simultaneously. The system state is as follows:

$$\delta \mathbf{x} = \left[ \delta \mathbf{x}_L^T \quad \delta \mathbf{x}_R^T \right]^T. \quad (9)$$

The discrete-time system dynamics model of a dual-foot pedestrian system is given as follows:

$$\delta \mathbf{x}_k = \Phi_{k,k-1} \delta \mathbf{x}_{k-1} + \mathbf{w}_{k-1} \quad (10)$$

$$\Phi_{k,k-1} = \begin{bmatrix} \Phi_{k,k-1}^L & \mathbf{0}_{15 \times 15} \\ \mathbf{0}_{15 \times 15} & \Phi_{k,k-1}^R \end{bmatrix}; \quad \mathbf{w}_{k-1} = \begin{bmatrix} \mathbf{w}_{k-1}^L \\ \mathbf{w}_{k-1}^R \end{bmatrix} \quad (11)$$

where superscripts  $L$  and  $R$  represent the state information related to the left and right foot, respectively. Obviously, the system noise  $\mathbf{w}_k$  still obey the Gaussian noise distribution with zero mean and covariance matrix  $\mathbf{Q}_k$ .

Once any of the two feet are detected in the stance phase by the SPD method described in Section III-B, the zero velocity can be used as an independent observation with zero mean white noise. Thus, it can be used to correct the dual-foot pedestrian system. The ZUPT model in the dual-foot pedestrian system is given as follows:

$$\begin{cases} \hat{\mathbf{v}}_{L,k}^n = [\mathbf{H}_0 \ \mathbf{0}_{3 \times 15}] \delta \mathbf{x}_k + \boldsymbol{\varepsilon}_v; & \text{case 1} \\ \hat{\mathbf{v}}_{R,k}^n = [\mathbf{0}_{3 \times 15} \ \mathbf{H}_0] \delta \mathbf{x}_k + \boldsymbol{\varepsilon}_v; & \text{case 2} \\ \begin{bmatrix} \hat{\mathbf{v}}_{L,k}^n \\ \hat{\mathbf{v}}_{R,k}^n \end{bmatrix} = \begin{bmatrix} \mathbf{H}_0 & \mathbf{0}_{3 \times 15} \\ \mathbf{0}_{3 \times 15} & \mathbf{H}_0 \end{bmatrix} \delta \mathbf{x}_k + \begin{bmatrix} \boldsymbol{\varepsilon}_v \\ \boldsymbol{\varepsilon}_v \end{bmatrix}; & \text{case 3} \end{cases} \quad (12)$$

where  $\hat{\mathbf{v}}_{L,k}^n$  and  $\hat{\mathbf{v}}_{R,k}^n$  are the left and right foot velocities estimated by the INS at time  $t_k$ , respectively;  $\mathbf{H}_0 = [\mathbf{0}_{3 \times 3} \ \mathbf{I}_{3 \times 3} \ \mathbf{0}_{3 \times 9}]$  is the basic measurement matrix; “case 1” and “case 2” represent the cases where the left and right foot are detected in the stance phase, respectively; “case 3” represents the case where both feet are in the stance phase; and  $\boldsymbol{\varepsilon}_v$  is the measurement noises, its covariance matrix  $\mathbf{R} = E[(\boldsymbol{\varepsilon}_v \boldsymbol{\varepsilon}_v^T)]$  is set to  $\text{diag}[(0.03)_{3 \times 1}^2]$ .

#### D. Proposed Minimum Distance Constraint Algorithm

Although the ZUPT algorithm has been used to correct the cumulative error in INS, the position error still cannot be eliminated due to the unobservable heading error effect. Regular distance changing information between the left and right foot has been widely demonstrated to enhance autonomous pedestrian positioning capability [31], [35], [36]. The positioning performance and robustness of the minimum distance-based solution are better than the maximum distance-based solution. This is mainly because the fluctuation of the minimum distance is smaller in various walking speeds and pattern scenarios. Therefore, this study uses the minimum distance as an independent constraint to improve the autonomous pedestrian positioning capability.

In traditional approaches, the known pseudo-observation algorithm is often used to deal with the optimal state estimation under the MDC [36]. First, the minimum distance is considered an additional observation and is incorporated into the ZUPT model to construct an augmented measurement equation. Then, the nonlinear Kalman filtering algorithm (e.g., EKF, UKF, and CKF) is used to implement the navigation state estimation. However, the traditional method does not fully exploit the improvement of the MDC on the positioning performance because of the solid nonlinear characteristic of the MDC information. Therefore, we propose an IDC algorithm to obtain an accurate and consistent state estimate in the dual-foot pedestrian positioning system.

The estimated distance  $\bar{d}_m$  between the left and right foot at the minimum distance moment  $t_m$  is given as follows:

$$\bar{d}_m = \|\bar{\mathbf{r}}_{L,m}^n - \bar{\mathbf{r}}_{R,m}^n\| \quad (13)$$

where  $\bar{\mathbf{r}}_m^* = \hat{\mathbf{r}}_m^n - \delta \mathbf{r}_m^n$  is the position after the ZUPT correction;  $\hat{\mathbf{r}}_m^n$  is foot position estimated by the INS;  $\delta \mathbf{r}_m^n$  is the estimated

position error by KF; and superscripts  $L$  and  $R$  represent the state information related to the left and right foot, respectively.

Although the fluctuation of the minimum distance between the left and right foot is relatively stable, it will inevitably be smaller than the stable constant minimum distance due to the irregular walking pattern such as cross-step. Thus, the IDC method is performed only when  $\bar{d}_m$  is greater than  $c_0$  ( $\bar{d}_m > c_0$ ), where  $c_0$  is the set threshold and is measured during the initial stationary standing phase. The state estimation under the distance constraint in the dual-foot pedestrian system can be formulated as the following optimization problem:

$$\tilde{\mathbf{x}}_m = \arg \min_{\tilde{\mathbf{x}}_m} (\tilde{\mathbf{x}}_m - \bar{\mathbf{x}}_m)^T \mathbf{W}_m (\tilde{\mathbf{x}}_m - \bar{\mathbf{x}}_m) \quad (14)$$

$$\text{s.t.} \quad \|\bar{\mathbf{r}}_{L,m}^n - \bar{\mathbf{r}}_{R,m}^n\|^2 - c_0^2 = 0 \quad (15)$$

where  $\mathbf{x}$  is the navigation state of the dual-foot pedestrian system and its error  $\delta \mathbf{x}$  is defined in (9);  $\tilde{\mathbf{x}}_m$  is the constrained estimate of  $\mathbf{x}_m$ ;  $\bar{\mathbf{x}}_m$  is an optimization variable of  $\mathbf{x}_m$ ;  $\bar{\mathbf{x}}_m$  is the estimate by the ZUPT algorithm and KF;  $\mathbf{W}_m = \mathbf{P}_m^{-1}$  is the weighting matrix,  $\mathbf{P}_m$  is the estimated covariance matrix by KF; and  $\mathbf{r}_L^n = \mathbf{x}_{1:3}$  and  $\mathbf{r}_R^n = \mathbf{x}_{16:18}$  are the position state of the left and right foot.

The distance constraint between the left and right foot in (15) can be rewritten as follows:

$$\mathbf{g}(\mathbf{x}_m) = \mathbf{x}_m^T \mathbf{M} \mathbf{x}_m - c_0^2 = 0 \quad (16)$$

$$\mathbf{M} = \begin{bmatrix} \mathbf{I}_{3 \times 3} & \mathbf{0}_{3 \times 12} & -\mathbf{I}_{3 \times 3} & \mathbf{0}_{3 \times 12} \\ \mathbf{0}_{12 \times 3} & \mathbf{0}_{12 \times 12} & \mathbf{0}_{12 \times 3} & \mathbf{0}_{12 \times 12} \\ -\mathbf{I}_{3 \times 3} & \mathbf{0}_{3 \times 12} & \mathbf{I}_{3 \times 3} & \mathbf{0}_{3 \times 12} \\ \mathbf{0}_{12 \times 3} & \mathbf{0}_{12 \times 12} & \mathbf{0}_{12 \times 3} & \mathbf{0}_{12 \times 12} \end{bmatrix}. \quad (17)$$

We suppose that the optimized navigation state  $\mathbf{x}_m$  contains an approximate estimate  $\bar{\mathbf{x}}_m$ . In that case, the distance constraint function  $\mathbf{g}(\mathbf{x}_m)$  can be expanded by the Taylor series expansion around the approximate estimate  $\bar{\mathbf{x}}_m$  as follows:

$$\mathbf{g}(\mathbf{x}_m) \approx \mathbf{g}(\bar{\mathbf{x}}_m) + 2\bar{\mathbf{x}}_m^T \mathbf{M} (\mathbf{x}_m - \bar{\mathbf{x}}_m) = \mathbf{A} \mathbf{x}_m - \mathbf{b} \quad (18)$$

where  $\mathbf{A} = 2\bar{\mathbf{x}}_m^T \mathbf{M}$ , and  $\mathbf{b} = 2\bar{\mathbf{x}}_m^T \mathbf{M} \bar{\mathbf{x}}_m - \mathbf{g}(\bar{\mathbf{x}}_m)$ .

Therefore, on the premise that an approximate estimate  $\bar{\mathbf{x}}_m$  is known, the distance constraint estimation in the dual-foot pedestrian system can be approximately formulated as the following linear optimization problem:

$$\tilde{\mathbf{x}}_m^* = \arg \min_{\tilde{\mathbf{x}}_m} (\tilde{\mathbf{x}}_m - \bar{\mathbf{x}}_m)^T \mathbf{W}_m (\tilde{\mathbf{x}}_m - \bar{\mathbf{x}}_m) \quad (19)$$

$$\text{s.t.} \quad \mathbf{A} \tilde{\mathbf{x}}_m - \mathbf{b} = 0 \quad (20)$$

where  $\tilde{\mathbf{x}}_m^*$  is the constrained estimate of  $\mathbf{x}_m$  in the presence of an approximate value  $\bar{\mathbf{x}}_m$ .

The nonlinear distance constraint can be converted into an approximate linear constraint problem when an approximate state estimate  $\bar{\mathbf{x}}_m$  is known. By following the basic idea of the estimation projection method [47], we projected the unconstrained estimate onto the approximate linear constrained surface. By using the Lagrange multiplier technique, the solution of the optimization problem in (19) and (20) can be obtained as follows:

$$\tilde{\mathbf{x}}_m^* = \bar{\mathbf{x}}_m - \mathbf{P}_m \mathbf{A}^T (\mathbf{A} \mathbf{P}_m \mathbf{A}^T)^{-1} (\mathbf{A} \bar{\mathbf{x}}_m - \mathbf{b}). \quad (21)$$

We can reasonably infer from (18)–(21) that the constrained estimate  $\check{\mathbf{x}}_m^*$  meets the distance constraint more than  $\bar{\mathbf{x}}_m$ . We assumed that the estimates  $\check{\mathbf{x}}_m^*$  and  $\bar{\mathbf{x}}_m$  both revolve around the true state  $\mathbf{x}_m$ . Based on this assumption, we replace the approximate estimate by the last constrained estimate, and deduce a series of alternative estimates through iteration updates. The most probable estimate is determined to be the final constrained estimate  $\check{\mathbf{x}}_m$ . In the normal walking scenario, the ZUPT-based pedestrian system has a considerable autonomous positioning ability (its accuracy usually is better than 5% of the walking distance), and its positioning error will not increase sharply. Therefore, the navigation state obtained by ZUPT in the dual-foot pedestrian system can be used as an initial approximate estimate, i.e.,  $\check{\mathbf{x}}_{m,0}^* = \bar{\mathbf{x}}_m$ . The iterative constrained estimate  $\check{\mathbf{x}}_{m,l+1}^*$  is given as follows:

$$\check{\mathbf{x}}_{m,l+1}^* = \bar{\mathbf{x}}_m - \mathbf{P}_m \mathbf{A}_l^T (\mathbf{A}_l \mathbf{P}_m \mathbf{A}_l^T)^{-1} (\mathbf{A}_l \bar{\mathbf{x}}_m - \mathbf{b}_l) \quad (22)$$

where  $\mathbf{A}_l = 2(\check{\mathbf{x}}_{m,l}^*)^T \mathbf{M}$ , and  $\mathbf{b}_l = 2(\check{\mathbf{x}}_{m,l}^*)^T \mathbf{M} \check{\mathbf{x}}_{m,l}^* - \mathbf{g}(\check{\mathbf{x}}_{m,l}^*)$ .

In each iteration update, the constrained covariance matrix  $\check{\mathbf{P}}_{m,l}$  is given as follows:

$$\begin{aligned} \check{\mathbf{P}}_{m,l+1} &= \mathbf{E} \left[ (\mathbf{x}_m - \check{\mathbf{x}}_{m,l+1}^*) (\mathbf{x}_m - \check{\mathbf{x}}_{m,l+1}^*)^T \right] \\ &= \mathbf{E} \left[ \mathbf{J}_l (\mathbf{x}_m - \bar{\mathbf{x}}_m) (\mathbf{x}_m - \bar{\mathbf{x}}_m)^T \mathbf{J}_l^T \right] \\ &= \mathbf{J}_l \mathbf{P}_m \mathbf{J}_l^T \end{aligned} \quad (23)$$

where  $\mathbf{J}_l = \mathbf{I} - \mathbf{P}_m \mathbf{A}_l^T (\mathbf{A}_l \mathbf{P}_m \mathbf{A}_l^T)^{-1} \mathbf{A}_l$ .

We can obtain a series of estimates through iterative updates. The criterion for determining the optimal estimate  $\check{\mathbf{x}}_m$  is to minimize the function  $(\check{\mathbf{x}}_m - \bar{\mathbf{x}}_m)^T \mathbf{W}_m (\check{\mathbf{x}}_m - \bar{\mathbf{x}}_m)$ . The maximum number of iterations in the proposed IDC algorithm is set to 5 through numerous experimental analysis.

### E. Computational Complexity Analysis

We define the computational complexity  $\mathcal{O}$  as the number of basic mathematical operations (i.e., addition, subtraction, multiplication, and division). We used the most straightforward matrix multiplication and classic Gauss-Jordan elimination methods [48] to analyze the computational complexity of the IDC algorithm. For an  $n \times m$  matrix  $\mathbf{A}$ , an  $m \times p$  matrix  $\mathbf{B}$ , and an  $n \times n$  matrix  $\mathbf{C}$ , we have  $\mathcal{O}(\mathbf{A}^T) = nm$ ,  $\mathcal{O}(\mathbf{A}\mathbf{B}) = n(2m-1)p$ , and  $\mathcal{O}(\mathbf{C}^{-1}) = n^3$ .

The dimension of the system state  $\mathbf{x}$  is  $30 \times 1$ . Since the matrix  $\mathbf{M}$  is a sparse matrix with only 0, 1, and  $-1$ , the specific forms of the updated variables  $\mathbf{A}_l$  and  $\mathbf{b}_l$  in (22) can be simply calculated. Therefore, the computational complexity of the variables  $\mathbf{A}_l$  and  $\mathbf{b}_l$  in a single update process is as follows:

$$\mathcal{O}(\mathbf{A}_l) = 12, \quad \mathcal{O}(\mathbf{b}_l) = 24. \quad (24)$$

After updating  $\mathbf{A}_l$  and  $\mathbf{b}_l$ , we define  $\mathbf{C}_1 = \mathbf{A}_l^T$ ,  $\mathbf{C}_2 = \mathbf{P}_m \mathbf{C}_1$ ,  $\mathbf{C}_3 = \mathbf{A}_l \mathbf{C}_2$ ,  $\mathbf{C}_4 = \mathbf{C}_3^{-1}$ ,  $\mathbf{C}_5 = \mathbf{A}_l \bar{\mathbf{x}}_m - \mathbf{b}_l$ ,  $\mathbf{C}_6 = \mathbf{C}_4 \mathbf{C}_5$ ,  $\mathbf{C}_7 = \mathbf{C}_2 \mathbf{C}_6$ , and  $\mathbf{C}_8 = \bar{\mathbf{x}}_m - \mathbf{C}_7$ . The variable  $\mathbf{A}_l$  contains 24 zero elements. Thus, we derive

$$\begin{cases} \mathcal{O}(\mathbf{C}_1) = 6, & \mathcal{O}(\mathbf{C}_2) = 330, \quad \mathcal{O}(\mathbf{C}_3) = 11, \quad \mathcal{O}(\mathbf{C}_4) = 1 \\ \mathcal{O}(\mathbf{C}_5) = 24, \quad \mathcal{O}(\mathbf{C}_6) = 1, \quad \mathcal{O}(\mathbf{C}_7) = 30, \quad \mathcal{O}(\mathbf{C}_8) = 30. \end{cases} \quad (25)$$

The computational complexity of the IDC algorithm in one iteration in (22) is as follows:

$$\begin{aligned} \mathcal{O}(\check{\mathbf{x}}_{m,l}^*) &= \mathcal{O}(\mathbf{A}_l) + \mathcal{O}(\mathbf{b}_l) + \mathcal{O}(\mathbf{C}_1) + \mathcal{O}(\mathbf{C}_2) + \mathcal{O}(\mathbf{C}_3) \\ &\quad + \mathcal{O}(\mathbf{C}_4) + \mathcal{O}(\mathbf{C}_5) + \mathcal{O}(\mathbf{C}_6) + \mathcal{O}(\mathbf{C}_7) \\ &\quad + \mathcal{O}(\mathbf{C}_8) = 469. \end{aligned} \quad (26)$$

In addition,  $\mathbf{J}_l = \mathbf{I} - \mathbf{C}_2 \mathbf{C}_4 \mathbf{A}_l$ , we derive

$$\mathcal{O}(\mathbf{C}_2 \mathbf{C}_4 \mathbf{A}_l) = 210, \quad \mathcal{O}(\mathbf{J}_l) = 180. \quad (27)$$

The computational complexity of the constrained state covariance matrix in (23) is given as follows:

$$\begin{aligned} \mathcal{O}(\check{\mathbf{P}}_{m,l}) &= \mathcal{O}(\mathbf{J}_l) + \mathcal{O}(\mathbf{J}_l^T) + 2n^2(2n-1) \\ &= 180 + 204 + 106200 = 106584. \end{aligned} \quad (28)$$

By setting the number of iterations  $l$ , we express the computational complexity of the IDC algorithm  $\mathcal{O}_{\text{IDC}}$  as follows:

$$\mathcal{O}_{\text{IDC}} = l \times \mathcal{O}(\mathbf{J}_l) + \mathcal{O}(\check{\mathbf{P}}_{m,l}) = l \times 469 + 106584. \quad (29)$$

Note that the effect of zero elements in variables and matrices is considered in the proposed algorithm's computational complexity analysis. The IDC algorithm has a low-computational effort and does not incur a computational burden in practical applications.

## IV. MINIMUM DISTANCE MOMENT DETECTION

The minimum distance moment determination in each gait cycle is crucial for the proposed MDC method, i.e., determining  $t_m$  in Section III-D. In this section, we first review the limitations of the current methods. Then, we present a new phenomenon associated with the minimum distance between the left and right foot. Finally, a straightforward MDMD method is proposed.

### A. Current Distance Constraint Moment Detection Methods

In the classical maximum distance constraint method (“MaxDist”) [31], [35], the constraint algorithm is activated only when the estimated distance between the left and right foot exceeds a set upper bound and the time difference between the current and the nearest constraint events exceeds a set time interval. In our previous proposed MDC algorithm (“MinDist”) [36], the constraint moment is jointly determined by the minimum distance information of the historical buffer positions within one gait cycle, the time interval between two adjacent constraint events, and the initially set threshold.

The estimated error of the pedestrian position will inevitably increase in long-term walking scenarios. The constraint moment in the current methods is closely related to the recursive foot position with increasing error. The current approaches [31], [35], [36] may result in potentially serious inconsistencies between the estimated and the actual distance. This inconsistency becomes more pronounced as the walking distance increases, leading to potentially unreasonable and low robustness of the pedestrian positioning system. As shown in Fig. 4, after 400 s of continuous walking, the estimated distances between the left and right foot using the

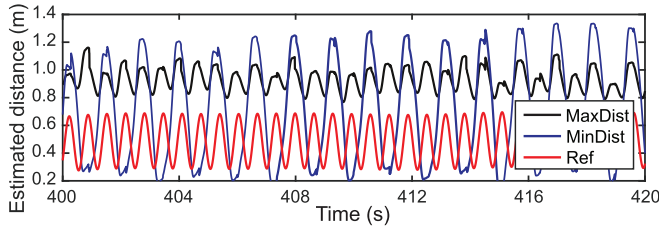


Fig. 4. Estimated distance between the left and right foot using the classical methods. The actual distance varies regularly in the range of 0.3–0.7 m.

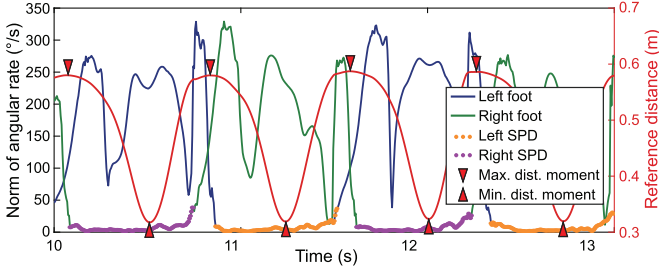


Fig. 5. Angular rate module and distance change between left and right foot in the dual-foot pedestrian system. A camera-based motion capture system provides the reference distance between the left and right foot.

classical methods are both unreasonable. The current methods may result in an under-utilized distance constraint, limiting its potential for positioning performance improvement.

### B. Minimum Distance Moment Phenomenon

In the dual-foot pedestrian system, the maximum distance moment corresponds to that when one foot just touches the ground (the specific force modulus at this moment rises to peak due to the strike of the fall to the ground). However, the minimum distance moment is difficult to determine. As shown in Fig. 5, the minimum distance moment is usually located within the stance phase of one foot while the other is in the swing phase. To explore the characteristics of the minimum distance change between the left and right foot, a minimum distance moment coefficient  $\kappa$  is defined as follows:

$$\kappa = (t_{\min} - t_{\text{fst}}) / (t_{\text{end}} - t_{\text{fst}}) \quad (30)$$

where  $t_{\text{fst}}$  and  $t_{\text{end}}$  are the start and end times of the stance phase, and  $t_{\min}$  is the minimum distance moment. Note that the durations  $t_{\min} - t_{\text{fst}}$  and  $t_{\text{end}} - t_{\text{fst}}$  vary with different step lengths, different pedestrians, and different walking speeds.

Based on careful observation and analysis, we notice that: *the minimum distance moment coefficient  $\kappa$  may fluctuate around a constant value in a normal walking scenario.* Therefore, we designed the following experimental tests to verify our speculation.

In the experimental tests, two inertial modules (described in Table I) were tightly mounted on the heels of the subject's left and right shoes, as shown in Fig. 1. Three subjects were instructed to walk 12 times at normal speed and gait pattern along a straight line trajectory. Each subject was asked to stand still for more than 30 s at the beginning and end of each test. The reference position of the left and right foot provided by a camera-based motion capture system.

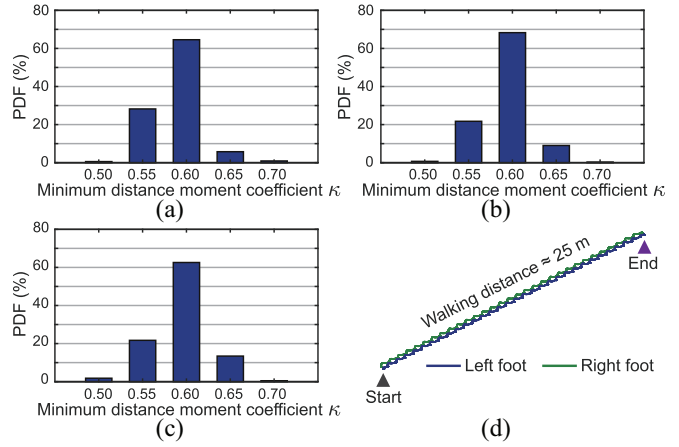


Fig. 6. Analysis of minimum distance moment coefficient  $\kappa$ . (a) Subject #1. (b) Subject #2. (c) Subject #3. (d) Reference trajectories.

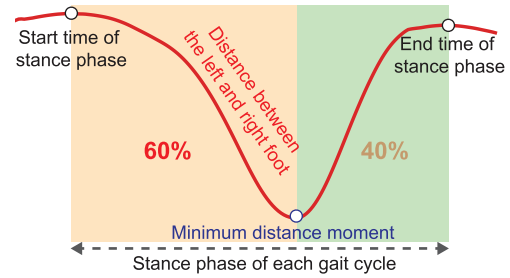


Fig. 7. Discovered new phenomenon associated with the minimum distance between the left and right foot.

The subject was approximately 37% in the stance phase during each gait cycle in the normal walking process, i.e., 75 epochs for the 200 Hz sampling frequency. Experimental analysis shows that the minimum distance moment coefficient  $\kappa$  fluctuates in the interval of 0.50–0.70. Therefore, we set five constant coefficients (0.50, 0.55, 0.60, 0.65, and 0.70) for statistical analysis. We calculate the probability distribution function (PDF) that the minimum distance moment coefficients of different subjects were located in five constant coefficient sets by the closest rule (e.g., the coefficients between 0.575 and 0.625 were counted into the 0.60 set).

As shown in Fig. 6, the experimental test results demonstrate that more than 60% of the minimum distance moment coefficients for the three subjects fell within the 0.60 group. Therefore, it is reasonable to believe that the minimum distance moment coefficient  $\kappa$  between the left and right feet of a pedestrian fluctuates around 0.60 in a normal walking scenario. Fig. 7 gives the discovered new phenomenon associated with the minimum distance between the left and right foot.

### C. Proposed MDMD Method

We propose an MDMD method by the discovered phenomenon in Section IV-B, the minimum distance moment coefficient  $\kappa$  is 0.60, and the moment  $t_{\min}$  is as follows:

$$t_{\min} = (1 - \kappa) \times t_{\text{fst}} + \kappa \times t_{\text{end}}. \quad (31)$$

The proposed method needs to be delayed for approximately half the gait cycle. Since the influence of the short delay time

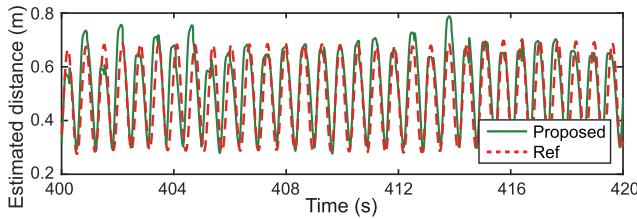


Fig. 8. Estimated distance using the proposed MDMD method.

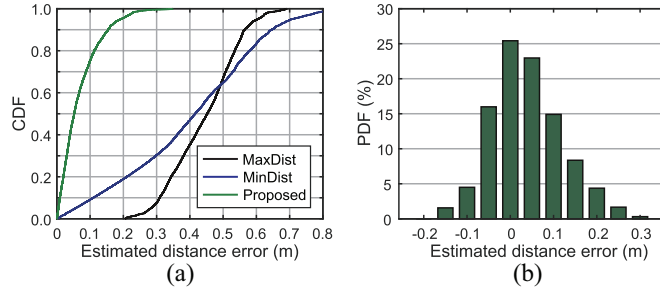


Fig. 9. Distance error distributions obtained by different methods in the statistical tests. (a) Cumulative distribution function (CDF) of the estimated distance error. (b) PDF of the distance error using the proposed method.

TABLE II  
ERROR STATISTICS OF ESTIMATED DISTANCE BETWEEN THE LEFT AND RIGHT FOOT USING DIFFERENT METHODS (m)

Method	Mean	RMS	MAX	Std
MaxDist	0.44	0.46	0.69	0.10
MinDist	0.22	0.45	0.88	0.39
Proposed	<b>0.04</b>	<b>0.09</b>	<b>0.35</b>	<b>0.08</b>

on the real-time positioning is weak (about  $0.5 * 75/200 = 0.1875$  s), we do not adopt any time delay processing strategy such as the delayed KF algorithm. The proposed MDMD method requires only the time information at the start and end of the stance phase in each gait cycle. Since the minimum distance moment coefficient is a ratio, the detection method can theoretically obtain the same results at different SPD thresholds. In this study, we use the SPD method in Section III-B to obtain the start time  $t_{\text{fst}}$  and end time  $t_{\text{end}}$ .

We compared the proposed MDMD method to the classical methods in [31] and [36]. Fig. 8 shows the estimated distance by the proposed MDMD method, and the distance error distributions obtained by different methods in the statistical tests are given in Fig. 9. Table II summarizes the distance error statistics, where Mean, RMS, MAX, and Std represent the mean, root mean square, maximum, and standard deviation, respectively.

Compared to the MaxDist method, the RMS and Std of the distance estimation error of the proposed method are reduced by 80% and 20%, respectively. Compared to the MinDist method, the RMS and Std of the distance estimation error of the proposed method are reduced by 80% and 79%, respectively. Therefore, the proposed MDMD method has higher accuracy, more reasonable, and more stable distance estimation in the dual-foot pedestrian positioning system than the classical methods. In the following experimental section, we shall

### Algorithm 1 Proposed Novel Enhanced MDC Method for the Dual-Foot Pedestrian Positioning System

**input:** inertial sensor data  $f_{ib}^b$  and  $\omega_{ib}^b$ , initial navigation and KF filter state, and minimum distance threshold  $c_0$ .

**output:** navigation state and corresponding covariance matrix.

- 1: **for**  $k = 1:n$  **do**
- 2: update navigation state by Section III-A, time update process of KF using the dynamic model in (10), and detect stance phase by Section III-B.
- 3: **if** any one of the two feet is in the stance phase **then**
- 4: measurement update of KF using the ZUPT model in (12), error feedback of KF.
- 5: **if** minimum distance moment is detected in Section IV-C, and  $\bar{d}_m > c_0$  **then**
- 6: set:  $\check{x}_{m,0}^* = \check{x}_m$ ,  $W_m = P_m^{-1}$ , and  $l = 1$ .
- 7: **while**  $l \leq 5$  **do**
- 8: calculate the iterative constrained estimate using (22), (23) and update  $l = l + 1$ .
- 9: **end while**
- 10: determine the optimal estimate  $\check{x}_m$  and covariance matrix  $P_m$ , update navigation state, and update covariance matrix  $P_m = \check{P}_m$  of KF.
- 11: **end if**
- 12: **end if**
- 13: **end for**

further demonstrate the improvement of the proposed MDMD method for pedestrian positioning performance.

The detailed implementation of the proposed novel enhanced MDC method for the dual-foot pedestrian positioning system is summarized in Algorithm 1.

## V. EXPERIMENTAL RESULTS

### A. Experimental Description

In order to evaluate the improvement of the proposed novel MDC method on the positioning performance of the dual-foot pedestrian system, we have conducted two experimental tests under rigorous scenarios with a walking trajectory of about 1000 m without turn around and closed loop. The long-distance walking trajectory without turn around and closed loop helps to objectively and genuinely reflect the autonomous pedestrian positioning performance. In addition, the straight-line constraint and building direction-assisted (e.g., heuristic drift elimination) algorithms may not meet their hypothesis condition and fail in challenging practical applications.

The two experimental test regions were located in the outdoor open sky area in December 2021 in Wuhan City. The reference trajectories of the experimental tests are shown in Fig. 10, which were provided with a post-processed kinematic carrier-phase differential GNSS (POST-RTK) technique. The positioning accuracy of the POST-RTK technique in the open sky scenario is approximately 0.05 m. The multi-antenna GNSS receiver was mounted on the back of the tester. Considering the difference between the back and the foot, the accuracy of the reference trajectories was better than 0.5 m.

To verify the effectiveness of the proposed MDC method in the dual-foot pedestrian positioning system, we compared the following seven methods: 1) ZUPT algorithm; 2) classic maximum distance constraint algorithm

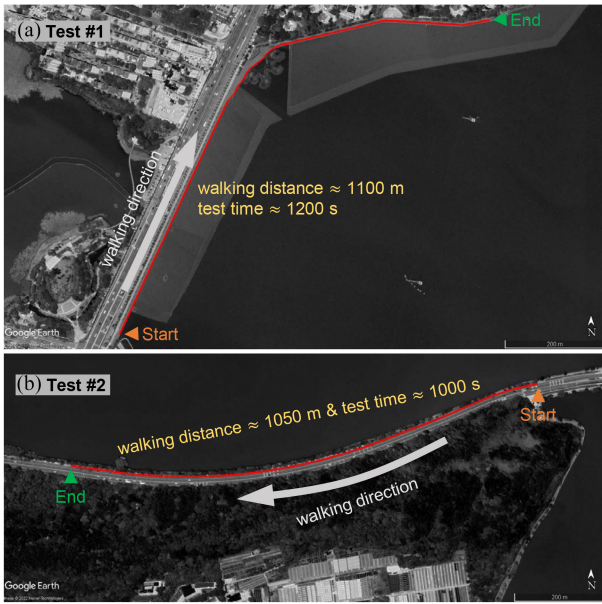


Fig. 10. Ground reference trajectories of the two experimental tests. (a) Test #1. (b) Test #2.

(MaxDist) [31]; 3) classic MDC algorithm (MinDist) [36]; 4) proposed MDMD + EKF-based pseudo-observation constraint algorithm [27] (“Our\_01”); 5) proposed MDMD + UKF-based pseudo-observation constraint algorithm [37], [38] (“Our\_02”); 6) proposed MDMD + CKF-based pseudo-observation constraint algorithm [39], [40] (“Our\_03”); and 7) proposed MDC method (“Our\_04”).

The experimental parameter settings were the same for the seven methods. The initial system covariance matrix  $P_0$  and the system noise matrix  $Q_k$  can be set by Table I, and the minimum distance threshold  $c_0$  is set 0.3 m by the experimental analysis result in [36]. The POST-RTK technique provided the initial position, the initial velocity was zero vector, and the initial roll and pitch angles were determined by standing still for a few seconds [45]. Moreover, we used two reference points to determine the initial yaw angle [43]: the first  $(r_{s,1}^x, r_{s,1}^y)$  is the initial position, and the second  $(r_{s,2}^x, r_{s,2}^y)$  is a reference point 10 m away from the first point. The initial yaw angle  $\psi_s$  is given as follows:

$$\psi_s = \arctan\left(\frac{r_{s,2}^y - r_{s,1}^y}{r_{s,2}^x - r_{s,1}^x}\right) - \arctan\left(\frac{\hat{r}_{s,2}^y - \hat{r}_{s,1}^y}{\hat{r}_{s,2}^x - \hat{r}_{s,1}^x}\right) \quad (32)$$

where  $s \in \{L, R\}$ , and  $L$  and  $R$  represent the state information related to the left and right foot, respectively; and  $(\hat{r}_{s,2}^x, \hat{r}_{s,2}^y)$  is the estimated position by ZUPT and KF.

### B. Positioning Performance of Different Algorithms

Figs. 11 and 12 show the estimated position trajectories using seven methods in experimental tests #1 and #2, respectively. Figs. 13 and 14 show the uncertainty of the north position error and heading error in experimental test #1, respectively. As can be seen in Figs. 13 and 14, the other six distance constraint algorithms achieve lower uncertainties in position and heading errors compared to the ZUPT algorithm. The

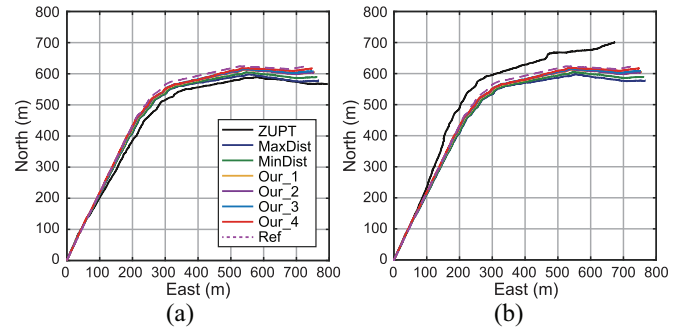


Fig. 11. Estimated trajectories using different methods in test #1. (a) Left foot. (b) Right foot.

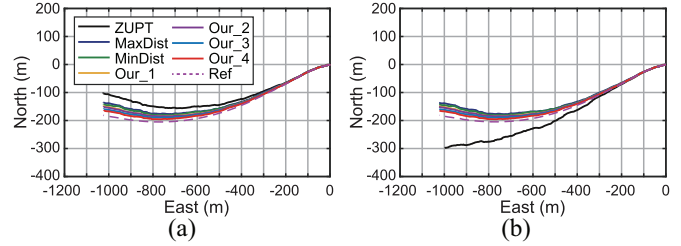


Fig. 12. Estimated trajectories using different methods in test #2. (a) Left foot. (b) Right foot.

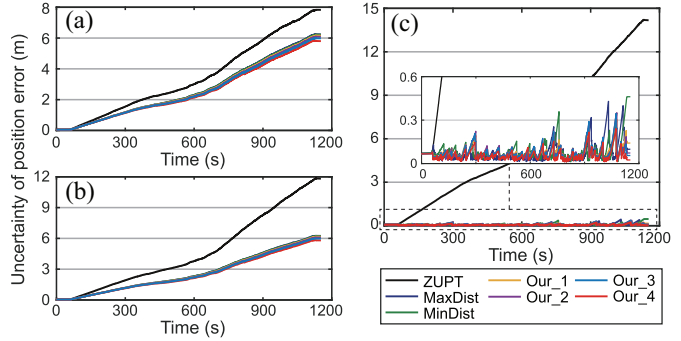


Fig. 13. Uncertainty of the north position estimation error obtained by different methods in experimental test #1, which is the root of the diagonal element of the estimated covariance matrix. (a) Left foot,  $\sqrt{P_{1,1}}$ . (b) Right foot,  $\sqrt{P_{16,16}}$ . (c) Relative position error,  $\sqrt{P_{1,1} + P_{16,16} - 2P_{1,16}}$ .

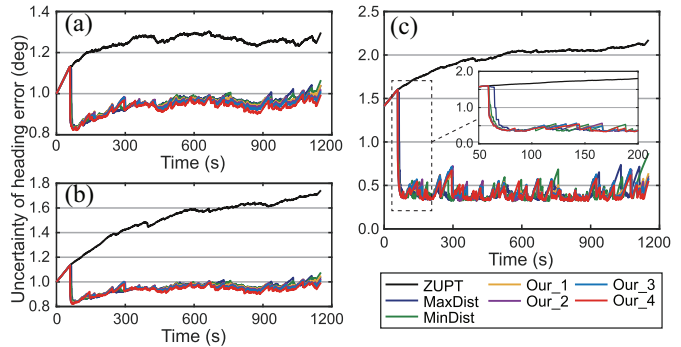


Fig. 14. Uncertainty of heading estimation error obtained by different methods in experimental test #1. (a) Left foot,  $\sqrt{P_{9,9}}$ . (b) Right foot,  $\sqrt{P_{24,24}}$ . (c) Relative heading error,  $\sqrt{P_{9,9} + P_{24,24} - 2P_{9,24}}$ .

experimental result proves that the distance constraint between the left and right foot improves the state estimation accuracy of the KF, which is beneficial for further improving the

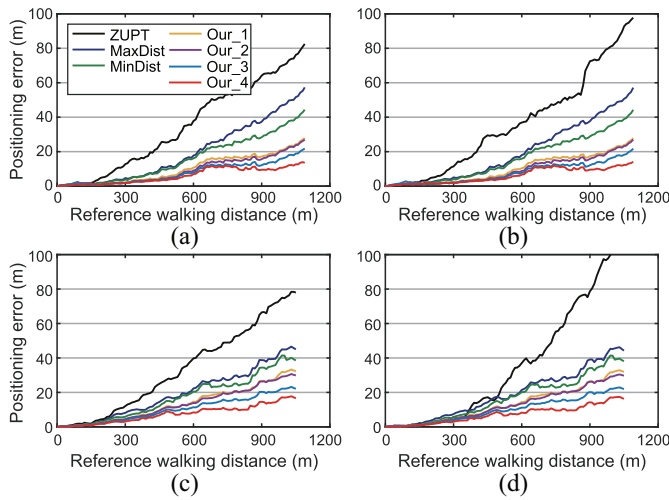


Fig. 15. Positioning error using different methods in experimental tests. (a) Left foot in test #1. (b) Right foot in test #1. (c) Left foot in test #2. (d) Right foot in test #2.

autonomous pedestrian positioning performance. In addition, the uncertainty of the relative heading error and the relative position error in the six distance constraint algorithms is convergent and smooth, instead of gradually diverging as in the ZUPT algorithm. That is, the introduction of the distance constraint transforms the relative heading and position states between the left and right foot in the dual-foot pedestrian system from unobservable to observable under the Kalman filtering framework, and it also validates the theoretical analysis in [27]. Therefore, the distance constraint between the left and right foot significantly improves the observability, state estimation accuracy, and positioning performance of the dual-foot pedestrian system.

The positioning error variations with increasing walking distance in the two experimental tests are given in Fig. 15. We also statistically analyzed the positioning errors of different walking distances using the seven methods in the two experimental tests. The statistical results are listed in Table III. It can be seen that the average positioning accuracy (i.e., position error drift rate) of the ZUPT algorithm decreases from 2.07% (200 m) to 8.2% (1000 m). The result indicates that the positioning error in the ZUPT algorithm increases curvilinearly with the walking distance rather than simply linearly. These nonlinear positioning error divergence characteristics of the ZUPT method were also analyzed theoretically in [18]. Note that since the ground is flatter indoors than outdoors, the pedestrian system has the same or better positioning performance in indoor environments.

As shown in Figs. 11(b), 12(b), and 15(b) and (d), the pedestrian position estimated by the ZUPT method has a large uncertainty due to the residual gyroscope bias effect, which may cause the positioning error to diverge faster. In the other six distance constraint methods, the mutual constraint of the left and right foot makes the relative gyroscope bias in the dual-foot system can be estimated, which reduces the estimation uncertainty and improves the positioning accuracy.

The minimum distance between the left and right foot is more stable and robust than the maximum distance

TABLE III  
POSITIONING ERROR STATISTICS AT DIFFERENT WALKING DISTANCES USING DIFFERENT METHODS IN EXPERIMENTAL TESTS (m)

Test	Method	200 m	400 m	600 m	800 m	1000 m	End*	
Test #1 Left foot	ZUPT	5.07	17.4	37.81	55.3	70.47	82.52	
	MaxDist	1.94	7.15	17.73	32.35	47.21	57.31	
	MinDist	1.79	6.73	16.13	25.66	35.28	44.33	
	Our_01	1.01	3.96	10.72	16.74	21.38	27.98	
	Our_02	<b>0.92</b>	3.27	9.05	14.83	20.79	27.01	
Test #1 Right foot	Our_03	0.98	3.09	8.04	12.14	16.36	21.83	
	Our_04	1.08	<b>2.82</b>	<b>6.95</b>	<b>9.65</b>	<b>11.01</b>	<b>13.52</b>	
	ZUPT	4.80	19.67	36.90	50.04	81.51	97.77	
	MaxDist	2.23	7.53	18.05	32.88	46.77	57.16	
	MinDist	1.89	6.95	15.92	26.12	35.60	44.28	
Test #2 Left foot	Our_01	<b>1.12</b>	3.99	10.40	16.94	21.66	27.83	
	Our_02	1.16	3.34	8.75	14.99	20.95	27.02	
	Our_03	1.19	3.17	7.78	12.40	16.56	21.75	
	Our_04	1.46	<b>3.02</b>	<b>6.70</b>	<b>9.73</b>	<b>11.33</b>	<b>14.10</b>	
	Test #2 Right foot	ZUPT	4.44	19.28	39.75	52.92	74.67	77.94
MaxDist		3.39	10.96	22.33	28.75	44.90	44.98	
MinDist		2.96	9.21	20.49	23.96	41.34	38.57	
Our_01		2.40	7.34	14.61	20.01	31.70	32.29	
Our_02		2.22	6.95	13.85	20.10	29.33	29.85	
Test #2 Left foot	Our_03	2.08	6.09	11.41	15.29	22.16	22.11	
	Our_04	<b>1.73</b>	<b>5.26</b>	<b>8.45</b>	<b>9.64</b>	<b>16.97</b>	<b>16.58</b>	
	Test #2 Right foot	ZUPT	2.30	13.78	37.11	65.45	100.95	117.17
		MaxDist	3.67	11.55	21.52	27.91	45.19	44.24
		MinDist	2.75	9.12	20.25	23.61	41.34	38.12
Our_01		2.22	7.22	14.45	19.82	31.66	31.97	
Our_02		2.04	6.73	13.61	19.85	29.25	29.72	
Test #2 Left foot	Our_03	1.89	5.87	11.18	14.99	22.08	21.94	
	Our_04	<b>1.62</b>	<b>5.13</b>	<b>8.29</b>	<b>9.41</b>	<b>16.94</b>	<b>16.27</b>	

\* Walking distance in experimental test #1 and test #2 were approximately 1100 m, and 1050 m, respectively.

information. Therefore, the method MinDist has better positioning performance than the MaxDist. The average positioning errors of the two classic methods in the test #1 (1100 m) were 5.2% and 4.0%, respectively. The average positioning errors of the two methods in the test #2 (1050 m) were 4.2% and 3.6%, respectively. Compared to method MaxDist, method MinDist improves positioning performance by approximately 19% in the two experimental tests.

The average positioning errors of the Our\_01 method in the two experimental tests were 2.54% (1100 m) and 3.06% (1050 m), respectively, which improved the positioning performance by 26% compared to the MinDist method. The experimental test results also demonstrate the reasonableness of the proposed MDMD method and its effectiveness in improving the autonomous pedestrian positioning performance.

Methods Our\_02 and Our\_03 use the pseudo-observation algorithm similar to the Our\_01 method to achieve the distance constraint optimal estimation, but differ in the nonlinear KF selection. Methods Our\_01, Our\_02, and Our\_03 use the EKF, UKF, and CKF algorithms. In the two experimental tests, the positioning accuracy of the Our\_02 method was slightly higher than that of the Our\_01 method, due to the better nonlinear state estimation performance of UKF than EKF. Since the CKF has a more powerful nonlinear processing capability than the EKF and UKF [39], Method Our\_03 has a higher accuracy positioning capability than methods Our\_01 and

TABLE IV  
RUN TIME OF DIFFERENT METHODS IN EXPERIMENTAL TESTS (s)

Method	ZUPT	MaxDist	MinDist	Our_01	Our_02	Our_03	Our_04
Test #1	33.25	42.87	40.02	36.36	38.08	38.25	37.21
Test #2	26.27	34.58	32.97	30.23	32.97	32.56	31.23

Our\_02. The positioning errors of method Our\_03 in the two experimental tests were 1.98 % (1100 m) and 2.10 % (1050 m), respectively.

The Our\_04 method achieves the highest positioning accuracy in the two experimental tests with 1.26 % (1100 m) and 1.56 % (1050 m), respectively. Compared to the ZUPT, MinDist and Our\_01 methods, method Our\_04 improves the average positioning performance in the two experimental tests by 83.50 %, 62.9 %, and 49.6 %, respectively. The experimental results indicate that the proposed IDC algorithm can fully utilize the distance constraint information better than the pseudo-observation method, thus achieving better state estimation accuracy and positioning performance. Therefore, the proposed novel MDC method improves the positioning performance of the dual-foot pedestrian system.

The seven methods for the dual-foot pedestrian system were programmed on MATLAB 2020b and executed on a computer with AMD Ryzen 7 4800H CPU @2.90 GHz and 16-GB memory. Table IV summarizes the run time of the seven methods in the two experimental tests. Method MaxDist has a higher computational complexity for state estimation, and method MinDist requires caching and updating the position information of the previous step. Thus, the run time of these two methods is longer than that of the ZUPT method.

Since the proposed MDMD method only requires the start and end times of the stance phase, the running time of method Our\_01 is shorter than that of method MinDist. The experimental results also demonstrate that the proposed MDMD method in Section IV reduces the algorithm complexity for the dual-foot pedestrian system. Compared to methods Our\_02 and Our\_03, method Our\_04 has a shorter running time. Therefore, the proposed MDC method in Section III-D reduces the computational complexity compared to the UKF-based and CKF-based pseudo-observation constraint algorithm. Note that the inertial navigation, SPD, and the ZUPT-based KF algorithms account for most of the running time in the different methods, rather than the distance constraint algorithm.

### C. Parameter Analysis of the Proposed Method

In the proposed novel MDC method, the minimum distance moment coefficient  $\kappa$  was set to 0.60 according to the statistical analysis in Section IV. Fig. 6 indicates that more than 20 % of the coefficients still fluctuate around 0.55 and 0.65. Therefore, we further analyzed the positioning performance of the proposed method (Our\_03) under the three minimum distance moment coefficient settings (0.55, 0.60, and 0.65) in experimental test #1. Figs. 16 and 17 show the estimated trajectories and positioning errors obtained by the proposed method under the three minimum distance moment coefficient settings, respectively. The positioning error statistics with different walking distances are summarized in Table V.

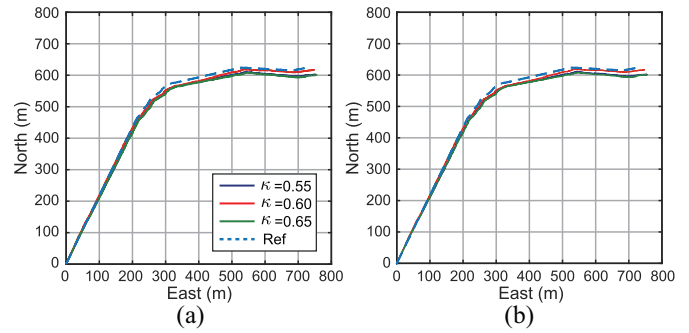


Fig. 16. Estimated trajectories of the proposed method with three minimum distance moment coefficients in experimental test #1. (a) Left foot. (b) Right foot.

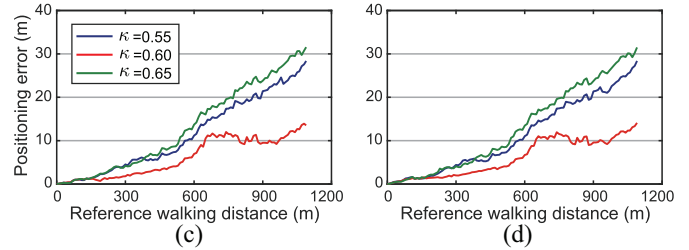


Fig. 17. Positioning error of the proposed method with three minimum distance moment coefficient settings in experimental test #1. (a) Left foot. (b) Right foot.

TABLE V  
POSITIONING ERROR STATISTICS OF THE PROPOSED METHOD WITH THREE MINIMUM DISTANCE MOMENT COEFFICIENTS (m)

Test #1	Scheme	200 m	400 m	600 m	800 m	1000 m	1100 m
Left foot	$\kappa = 0.55$	2.28	5.44	11.18	18.67	23.53	28.37
	$\kappa = 0.60$	1.08	2.82	6.95	9.65	11.01	13.52
	$\kappa = 0.65$	2.38	6.50	13.70	22.08	27.97	31.55
Right foot	$\kappa = 0.55$	1.89	5.30	11.04	18.74	23.50	28.38
	$\kappa = 0.60$	1.46	3.02	6.7	9.73	11.33	14.10
	$\kappa = 0.65$	2.16	6.43	13.47	22.07	27.95	31.49

The average positioning errors of the proposed method were approximately 2.58 %, 1.26 %, and 2.87 % for the three minimum distance moment coefficient setting schemes, respectively. The positioning performance of the second scheme (i.e.,  $\kappa = 0.60$ ) was approximately twice as good as the other two schemes. The experimental results further demonstrate the phenomenon that the minimum distance moment coefficient  $\kappa$  between the left and right foot fluctuates around 0.60 in a normal walking scenario.

In addition, we analyzed the effect of the SPD threshold on the positioning performance in the proposed method. We set three different thresholds to detect the minimum distance moment  $t_{\min}$  in the experimental test #1, i.e., to obtain the start time  $t_{\text{fst}}$  and end time  $t_{\text{end}}$  in (31). The three thresholds have been set to 6000, 8000, and 10000, respectively. Note that the different SPD thresholds have a significant impact on the ZUPT algorithm. For a fair comparison, we only analyze the effect of different thresholds on the proposed MDMD method. The SPD threshold of the ZUPT algorithm remained the same in the three schemes. Fig. 18 shows the positioning errors of

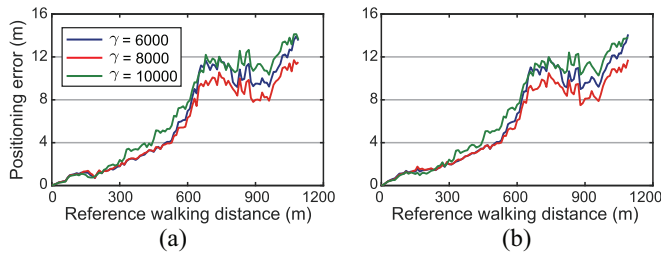


Fig. 18. Positioning error of the proposed method under three SPD thresholds in experimental test #1. (a) Left foot. (b) Right foot.

TABLE VI  
POSITIONING ERROR STATISTICS OF THE PROPOSED METHOD WITH  
THREE DIFFERENT SPD THRESHOLDS (m)

Test #1	Scheme	200 m	400 m	600 m	800 m	1000 m	1100 m
Left foot	$\gamma = 6000$	1.08	2.82	6.95	9.65	11.01	13.52
	$\gamma = 8000$	1.11	2.88	6.33	9.02	10.03	11.54
	$\gamma = 10000$	1.05	3.80	7.70	10.72	12.19	13.62
Right foot	$\gamma = 6000$	1.46	3.02	6.70	9.73	11.33	14.10
	$\gamma = 8000$	1.49	3.03	6.69	9.15	10.13	11.75
	$\gamma = 10000$	1.23	3.78	7.43	10.78	12.45	13.79

the proposed algorithm with the three SPD threshold settings, and Table VI summarizes the positioning error statistics with different walking distances.

The average positioning errors of the proposed method were approximately 1.26 %, 1.06 %, and 1.25 % for the three SPD threshold settings, respectively. The maximum difference in position error among the three schemes was approximately 2.4 m (1100 m walking distance). Considering the normal numerical fluctuations in the SPD algorithm, we can conclude that the proposed MDMD method is almost immune to the SPD threshold. The experimental test results under different SPD threshold settings also demonstrate the robustness of the proposed MDC method in the dual-foot pedestrian system.

## VI. CONCLUSION AND FUTURE WORK

This article presents a novel enhanced MDC method for the dual-foot pedestrian positioning system. The proposed method achieves superior positioning performance compared to traditional methods by making more reasonable use of the distance constraint information. First, an IDC algorithm is proposed to reduce nonlinear error losses, thus maximizing the improvement of autonomous positioning performance to obtain accurate and consistent state estimates under nonlinear MDCs. Second, a more reasonable and stable MDMD is designed based on a discovered phenomenon (i.e., the minimum distance moment coefficient fluctuates around the constant value of 0.60 in a normal walking scenario). The MDMD method overcomes the problem related to recursive position effects on distance constraint moment detection. Two rigorous experimental tests with a long walking trajectory without turn around and closed loop were conducted to verify the effectiveness of the proposed method. Experimental results demonstrated that the positioning performance of the proposed method was better than 1.5 % (walking distance over 1000 m)

and improved the positioning accuracy by 83.5 % and 62.9 % compared to the ZUPT method and the classical MDC method, respectively. Moreover, the experimental analysis further verifies the reasonability and robustness of the proposed method.

This article mainly considers the positioning performance that can be achieved by the dual-foot pedestrian system improved by the MDC in challenging positioning scenarios (that is, the user walks on non-straight-line and non-closed-loop routes). However, some valuable constraint information can still effectively improve the positioning performance in ordinary cases, such as straight-line constraints, closed-loop trajectories, etc. Therefore, we will consider combining the traditional constraint information with the proposed method in the next study. The MDC assumption in this article may be broken in complex walking scenarios (e.g., mountainous environments), and the proposed MDMD method is difficult to adapt to nonhealthy pedestrians (e.g., leg injuries). Therefore, we will consider using additional sensors to obtain more accurate and stable minimum distance and constraint moments to improve the stability of pedestrian positioning in practical applications in our future work. Furthermore, we also plan deeper investigations into the regular features of pedestrian motion to improve the capacity and stability of autonomous pedestrian positioning.

## REFERENCES

- [1] S. Wang, Q. Hu, Y. Sun, and J. Huang, "Privacy preservation in location-based services," *IEEE Commun. Mag.*, vol. 56, no. 3, pp. 134–140, Mar. 2018.
- [2] Y. Celik, S. Stuart, W. Woo, E. Sejdic, and A. Godfrey, "Multi-modal gait: A wearable, algorithm and data fusion approach for clinical and free-living assessment," *Inf. Fusion*, vol. 78, pp. 57–70, Feb. 2022.
- [3] S. Qiu et al., "Multi-sensor information fusion based on machine learning for real applications in human activity recognition: State-of-the-art and research challenges," *Inf. Fusion*, vol. 80, pp. 241–265, Apr. 2022.
- [4] S. Lee, B. Kim, H. Kim, R. Ha, and H. Cha, "Inertial sensor-based indoor pedestrian Localization with minimum 802.15.4a configuration," *IEEE Trans. Ind. Informat.*, vol. 7, no. 3, pp. 455–466, Aug. 2011.
- [5] R. Harle, "A survey of indoor inertial positioning systems for pedestrians," *IEEE Commun. Surveys Tuts.*, vol. 15, no. 3, pp. 1281–1293, 3rd Quart., 2013.
- [6] B. Zhou, Q. Li, Q. Mao, W. Tu, and X. Zhang, "Activity sequence-based indoor pedestrian localization using smartphones," *IEEE Trans. Human-Mach. Syst.*, vol. 45, no. 5, pp. 562–574, Oct. 2015.
- [7] Z. Chen, Q. Zhu, and Y. C. Soh, "Smartphone inertial sensor-based indoor localization and tracking with iBeacon corrections," *IEEE Trans. Ind. Informat.*, vol. 12, no. 4, pp. 1540–1549, Aug. 2016.
- [8] F. Zafari, A. Gkelias, and K. K. Leung, "A survey of indoor localization systems and technologies," *IEEE Commun. Surveys Tuts.*, vol. 21, no. 3, pp. 2568–2599, 3rd Quart., 2019.
- [9] G. Marta et al., "Wearable biofeedback suit to promote and monitor aquatic exercises: A feasibility study," *IEEE Trans. Instrum. Meas.*, vol. 69, no. 4, pp. 1219–1231, Apr. 2020.
- [10] R. Zhang, F. Hoflinger, and L. Reindl, "Inertial sensor based indoor localization and monitoring system for emergency responders," *IEEE Sensors J.*, vol. 13, no. 2, pp. 838–848, Feb. 2013.
- [11] A. F. G. G. Ferreira, D. M. A. Fernandes, A. P. Catarino, and J. L. Monteiro, "Localization and positioning systems for emergency responders: A survey," *IEEE Commun. Surveys Tuts.*, vol. 19, no. 4, pp. 2836–2870, 4th Quart., 2017.
- [12] X. Zhang et al., "Low-cost inertial measurement unit calibration with nonlinear scale factors," *IEEE Trans. Ind. Informat.*, vol. 18, no. 2, pp. 1028–1038, Feb. 2022.

- [13] C. Chen, C. X. Lu, J. Wahlström, A. Markham, and N. Trigoni, "Deep neural network based inertial odometry using low-cost inertial measurement units," *IEEE Trans. Mobile Comput.*, vol. 20, no. 4, pp. 1351–1364, Apr. 2021.
- [14] E. Foxlin, "Pedestrian tracking with shoe-mounted inertial sensors," *IEEE Comput. Graph. Appl.*, vol. 25, no. 6, pp. 38–46, Nov./Dec. 2005.
- [15] S. Chen, J. Lach, B. Lo, and G.-Z. Yang, "Toward pervasive gait analysis with wearable sensors: A systematic review," *IEEE J. Biomed. Health Inform.*, vol. 20, no. 6, pp. 1521–1537, Nov. 2016.
- [16] I. Skog, P. Handel, J.-O. Nilsson, and J. Rantakokko, "Zero-velocity detection—An algorithm evaluation," *IEEE Trans. Biomed. Eng.*, vol. 57, no. 11, pp. 2657–2666, Nov. 2010.
- [17] A. Ramanandan, A. Chen, and J. A. Farrell, "Inertial navigation aiding by stationary updates," *IEEE Trans. Intell. Transp. Syst.*, vol. 13, no. 1, pp. 235–248, Mar. 2012.
- [18] Y. Wang, A. Chernyshoff, and A. M. Shkel, "Study on estimation errors in ZUPT-aided pedestrian inertial navigation due to IMU noises," *IEEE Trans. Aerosp. Electron. Syst.*, vol. 56, no. 3, pp. 2280–2291, Jun. 2020.
- [19] A. Jiménez, F. Seco, J. Prieto, and J. Guevara, "Indoor pedestrian navigation using an INS/EKF framework for yaw drift reduction and a foot-mounted IMU," in *Proc. 7th Workshop Position, Navig. Commun.*, Mar. 2010, pp. 135–143.
- [20] J. Borenstein and L. Ojeda, "Heuristic drift elimination for personnel tracking systems," *J. Navig.*, vol. 63, no. 4, p. 591, 2010.
- [21] A. R. Jiménez, F. Seco, F. Zampella, J. C. Prieto, and J. Guevara, "Improved heuristic drift elimination (iHDE) for pedestrian navigation in complex buildings," in *Proc. Int. Conf. Indoor Position. Indoor Navig.*, Sep. 2011, pp. 1–8.
- [22] Z. Deng, P. Wang, T. Liu, Y. Cao, and B. Wang, "Foot-mounted pedestrian navigation algorithm based on BOR/MINS integrated framework," *IEEE Trans. Ind. Electron.*, vol. 67, no. 5, pp. 3980–3989, May 2020.
- [23] X. Niu, T. Liu, J. Kuang, Q. Zhang, and C. Guo, "Pedestrian trajectory estimation based on foot-mounted inertial navigation system for multi-story buildings in postprocessing mode," *IEEE Internet Things J.*, vol. 9, no. 9, pp. 6879–6892, May 2022.
- [24] M. Laverne, M. George, D. Lord, A. Kelly, and T. Mukherjee, "Experimental validation of foot to foot range measurements in pedestrian tracking," in *Proc. ION GNSS Conf.*, Sep. 2011, pp. 1386–1393.
- [25] J.-O. Nilsson, D. Zachariah, I. Skog, and P. Händel, "Cooperative localization by dual foot-mounted inertial sensors and inter-agent ranging," *EURASIP J. Adv. Signal Process.*, vol. 2013, p. 164, Oct. 2013. [Online]. Available: <https://doi.org/10.1186/1687-6180-2013-164>
- [26] D. Weenk, D. Roetenberg, B.-J. J. F. van Beijnum, H. J. Hermens, and P. H. Veltink, "Ambulatory estimation of relative foot positions by fusing ultrasound and inertial sensor data," *IEEE Trans. Neural Syst. Rehabil. Eng.*, vol. 23, no. 5, pp. 817–826, Sep. 2015.
- [27] M. Zhu, Y. Wu, and S. Luo, "i<sup>2</sup>IMU-R: Pedestrian navigation by low-cost foot-mounted dual IMUs and Interfoot ranging," *IEEE Trans. Control Syst. Technol.*, vol. 30, no. 1, pp. 247–260, Jan. 2022.
- [28] T. N. Hung and Y. S. Suh, "Inertial sensor-based two feet motion tracking for gait analysis," *Sensors*, vol. 13, no. 5, pp. 5614–5629, 2013.
- [29] A. Ahmed and S. Roumeliotis, "A visual-inertial approach to human gait estimation," in *Proc. IEEE Int. Conf. Robot. Autom. (ICRA)*, 2018, pp. 4614–4621.
- [30] C.-S. Jao, Y. Wang, and A. M. Shkel, "Pedestrian inertial navigation system augmented by vision-based foot-to-foot relative position measurements," in *Proc. IEEE/ION Position Location Navigat. Symp. (PLANS)*, 2020, pp. 900–907.
- [31] I. Skog, J.-O. Nilsson, D. Zachariah, and P. Händel, "Fusing the information from two navigation systems using an upper bound on their maximum spatial separation," in *Proc. Int. Conf. Indoor Positioning Indoor Navigat. (IPIN)*, 2012, pp. 1–5.
- [32] W. Shi, Y. Wang, and Y. Wu, "Dual MIMU pedestrian navigation by inequality constraint Kalman filtering," *Sensors*, vol. 17, no. 2, p. 427, 2017.
- [33] Q. Wang, M. Cheng, A. Noureldin, and Z. Guo, "Research on the improved method for dual foot-mounted inertial/magnetometer pedestrian positioning based on adaptive inequality constraints Kalman filter algorithm," *Measurement*, vol. 135, pp. 189–198, Mar. 2019.
- [34] H. Zhao et al., "Heading drift reduction for foot-mounted inertial navigation system via multi-sensor fusion and dual-gait analysis," *IEEE Sensors J.*, vol. 19, no. 19, pp. 8514–8521, Oct. 2019.
- [35] W. Zhang, D. Wei, H. Yuan, and G. Yang, "Cooperative positioning method of dual foot-mounted inertial pedestrian dead reckoning systems," *IEEE Trans. Instrum. Meas.*, vol. 70, 2021, Art. no. 8502114, doi: [10.1109/TIM.2021.3066173](https://doi.org/10.1109/TIM.2021.3066173).
- [36] X. Niu, Y. Li, J. Kuang, and P. Zhang, "Data fusion of dual foot-mounted IMU for pedestrian navigation," *IEEE Sensors J.*, vol. 19, no. 12, pp. 4577–4584, Jun. 2019.
- [37] G. Zhou, K. Li, X. Chen, L. Wu, and T. Kirubarajan, "State estimation with a destination constraint using pseudo-measurements," *Signal Process.*, vol. 145, pp. 155–166, Apr. 2018.
- [38] X. Tong et al., "A double-step unscented Kalman filter and HMM-based zero-velocity update for pedestrian dead reckoning using MEMS sensors," *IEEE Trans. Ind. Electron.*, vol. 67, no. 1, pp. 581–591, Jan. 2020.
- [39] C. Shen, Y. Zhang, J. Tang, H. Cao, and J. Liu, "Dual-optimization for a MEMS-INS/GPS system during GPS outages based on the cubature Kalman filter and neural networks," *Mech. Syst. Signal Process.*, vol. 133, Nov. 2019, Art. no. 106222.
- [40] C. Shen et al., "Seamless GPS/inertial navigation system based on self-learning square-root cubature Kalman filter," *IEEE Trans. Ind. Electron.*, vol. 68, no. 1, pp. 499–508, Jan. 2021.
- [41] C. Yang and E. Blasch, "Kalman filtering with nonlinear state constraints," *IEEE Trans. Aerosp. Electron. Syst.*, vol. 45, no. 1, pp. 70–84, Jan. 2009.
- [42] A. H. J. Ruiter, "Quadratically constrained least squares with aerospace applications," *J. Guid. Control Dyn.*, vol. 39, no. 3, pp. 487–497, 2016.
- [43] T. Liu, J. Kuang, W. Ge, P. Zhang, and X. Niu, "A simple positioning system for large-scale indoor patrol inspection using foot-mounted INS, QR code control points, and smartphone," *IEEE Sensors J.*, vol. 21, no. 4, pp. 4938–4948, Feb. 2021.
- [44] E.-H. Shin, "Estimation techniques for low-cost inertial navigation," Ph.D. dissertation, Dept. Geomatics Eng., Univ. Calgary, Calgary, AB, Canada, 2005.
- [45] X. Niu, T. Liu, J. Kuang, and Y. Li, "A novel position and orientation system for pedestrian indoor mobile mapping system," *IEEE Sensors J.*, vol. 21, no. 2, pp. 2104–2114, Jan. 2021.
- [46] Z. Wang, H. Zhao, S. Qiu, and Q. Gao, "Stance-phase detection for ZUPT-aided foot-mounted pedestrian navigation system," *IEEE/ASME Trans. Mechatronics*, vol. 20, no. 6, pp. 3170–3181, Dec. 2015.
- [47] D. Simon and T. L. Chia, "Kalman filtering with state equality constraints," *IEEE Trans. Aerosp. Electron. Syst.*, vol. 38, no. 1, pp. 128–136, Jan. 2002.
- [48] F. L. Gall, "Powers of tensors and fast matrix multiplication," in *Proc. 39th Int. Symp. Symbolic Algebr. Comput.*, 2014, pp. 296–303.



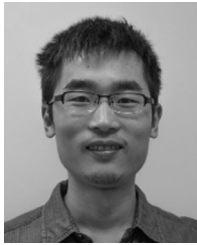
**Tao Liu** received the B.S. degree in geographic information system and the M.S. degree in surveying and mapping from Liaoning Technical University, Fuxin, China, in 2015 and 2018, respectively. He is currently pursuing the Ph.D. degree with the GNSS Research Center, Wuhan University, Wuhan, China.

His research interests focus on inertial navigation, multisensor fusion algorithm, IMU-based body sensor network, pedestrian navigation, and indoor positioning.



**Jian Kuang** received the B.Eng. degree and the Ph.D. degree in geodesy and survey engineering from Wuhan University, Wuhan, China, in 2013 and 2019, respectively.

He is currently a Postdoctoral Fellow with the GNSS Research Center, Wuhan University. His research interests focus on inertial navigation, pedestrian navigation, and indoor positioning.



**You Li** (Member, IEEE) received the B.Eng. degree from the China University of Geoscience (Beijing), Beijing, China, in 2009, the first Ph.D. degree from Wuhan University, Wuhan, China, in 2015, and the second Ph.D. degree from the University of Calgary, Calgary, AB, Canada, in 2016.

He is a Professor with the State Key Laboratory of Information Engineering in Surveying, Mapping and Remote Sensing, Wuhan University, where he is also an Adjunct Professor with Hubei LuoJia Laboratory. His research focuses on positioning and motion-

tracking techniques and applications. He has co-published over 100 academic papers and has over 20 patents pending.

Prof. Li serves as an Associate Editor for the *IEEE SENSORS JOURNAL*, a Committee Member at the International Association of Geodesy unmanned navigation system session, China Society of Surveying and Mapping location services session, the Secretary at the International Society for Photogrammetry and Remote Sensing mobile mapping session, and the co-chair of multiple international workshops or conferences.



**Xiaoji Niu** received the B.Eng. degree (with Hons.) in mechanical and electrical engineering and the Ph.D. degree from Tsinghua University, Beijing, China, in 1997 and 2002, respectively.

From 2003 to 2007, he was a Postdoctoral Fellow with the Mobile Multi-Sensor Systems Research Group, Department of Geomatics Engineering, University of Calgary, Calgary, AB, Canada. From 2007 to 2009, he was a Senior Scientist with SiRF Technology, Inc, San Jose, CA, USA. He is currently a Professor with the GNSS Research Center,

Artificial Intelligence Institute, Wuhan University, Wuhan, China, where he is also a Professor with Hubei LuoJia Laboratory. His research interests focus on INS and GNSS/INS integration for land vehicle navigation and pedestrian navigation.